Thermal Runaway Detection of Cylindrical 18650 Lithium-Ion Battery under Quasi-Static Loading Conditions

Muhammad Sheikh [a,*], Ahmed Elmarakbi [a], Mustafa Elkady [b],

[a] School of Engineering, Faculty of Engineering and advanced Manufacturing, University of Sunderland, St Peter's Campus, St Peter's Way, Sunderland, SR6 0DD, UK,

[b] Department of Mechanical Engineering, School of Engineering, Lebanese International University (LIU), Mouseitbeh - Beirut – Lebanon

[b] Department of Automotive Engineering, Faculty of Engineering, Ain Shams University, Cairo, Egypt

* Corresponding author: School of Engineering, Faculty of Engineering and advanced Manufacturing, University of Sunderland, St Peter's Campus, St Peter's Way, Sunderland, SR6 0DD, UK.

Email address: Muhammad.sheikh@research.sunderland.ac.uk (Muhammad Sheikh)

Abstract

This paper focuses on state of charge (SOC) dependent mechanical failure analysis of 18650 lithium-ion battery to detect signs of thermal runaway. Quasi-static loading conditions are used with four test protocols (Rod, Circular punch, three-point bend and flat plate) to analyse the propagation of mechanical failures and failure induced temperature changes. Finite element analysis (FEA) is used to model single battery cell with the concentric layered formation which represents a complete cell. The numerical simulation model is designed with solid element formation where stell casing and all layers followed the same formation, and fine mesh is used for all layers. Experimental work is also performed to analyse deformation of 18650 lithium-ion cell. The numerical simulation model is validated with experimental results. Deformation of cell mimics thermal runaway and various thermal runaway detection strategies are employed in this work including, force-displacement, voltage-temperature,

stress-strain, SOC dependency and separator failure. Results show that cell can undergo severe conditions even with no fracture or rupture, these conditions may slow to develop but they can lead to catastrophic failures. The numerical simulation technique is proved to be useful in predicting initial battery failures, and results are in good correlation with the experimental results.

1. Introduction

Batteries are becoming more and more essential to modern life as the world moves away from the non-sustainable use of fossil fuels. Therefore batteries are required to demonstrate good performance under diverse conditions. The safety and performance of lithium ion batteries are highly dependent upon the materials that are used to produce the batteries [1] as well as on the battery size, design, quality and energy content [2] [3]. Abuse of batteries to cause damage to batteries are carried out due to safety issues, especially when the deployment of the batteries is large [3-5]. Potential damages include cell rupture, release of debris (leakage) and test box damage [5]. Short circuit predictions are used as criteria for initial cell failures, but detail failure patterns and comparative analysis for battery degradation is rarely found in the available technical literature. In [6] modelling approach is used to predict short circuit under mechanical abuse, and available experimental results were used to verify the model. The quasi-static analysis was carried for the representative sandwich model, and scaled thicknesses of each battery component were used for complete battery model, this approach provides a good base to set different short circuit detection criterion but due to scaled thickness failure pattern may differ compare to real-time failure. In [7] short circuit of the battery is observed using two mechanical loading conditions including compression and bending, nominal stress-strain failure criteria are used; however simulation model to validate experimental work is not considered.

Assumptions based on past research were that the cell voltage could be used to identify the initiation of mechanical failure [8] [9]. Tension (stress: strain ratio) causes an initiation of cut-off [4][10]. Rigid rod indentation tests calibrate with hemispherical punch test results, so the hemispherical punch was not used in the current research as it was previously used by [11],

in [4], authors pointed out that observations of mechanical abuse to lithium ion batteries during experiments of cell voltage were useful for identifying the moment of mechanical failure. The moment a voltage drop occurred was the instant that structural, mechanical failure occurred [4]. “The short-circuit initiation was assumed to be co-located along the same coordinates at which the principal tensile stress first reaches a certain magnitude” [4].

In [11], authors carried out experiments to identify the cut-off stress and reported that tension causes a complex failure process. They reported that cut off stress occurs at 10 MPa, and identified as the tensile strength cut off. The tensile strength cut-off is assumed to be the value that controls the onset of a short circuit [11]. Cut-off stress largely depends on the battery material, operating and loading conditions of the battery.

In [6,7,11, 13,14, 20-23] different approaches are used to investigate short circuit of batteries where mechanical loading is used to perform abuse testing. In [11], four test protocols are used to investigate short circuit, similar test protocols are also used in [7] where standards given in [15] are followed, and in [16] similar techniques are used for simulation. Temperature variations are not considered in battery abuse failure, and is useful to predict battery degradation and short circuit; however sudden force and voltage drop are used as a failure of battery and initiation of the short circuit [9].

Short circuit leading to thermal runaway is not found in detail but extreme abuse conditions according to battery testing standards SAE, J2464 [15] is found in literature where nail penetration, oven test, crush test internal and external short circuits are used to evaluate thermal runaway and spreading of thermal runaway into adjacent cells [17][18].

To validate lithium-ion battery results, adoption of closest possible formation is important as the size of the battery and individual layer formation can play an important role to provide accurate results. Different numerical simulation techniques are found in the literature including representative sandwich (RS) model [6,20], representative volume element (RVE) model [21] and layered formation [11,22,23,27] for different types of lithium-ion batteries including pouch, prismatic and cylindrical cells. Element size selection and type of element is crucial in this regard for computational efficiency. Courant criterion for element edge length given in [23] is useful to estimate critical element edge length and time step calculations for this young's modulus and density of the material is required to estimate these values. Eq. (1) is used for this "l" is edge length of the element, □Δt is critical simulation time step, E is Young'' modulus, and ρ is the material density.

$$l = \Delta t \sqrt{\frac{E}{\rho}} \tag{1}$$

Material cards for different battery materials is also crucial to better represent battery simulation model, so commonly used material cards found in literature are MAT-63-CRUSHABLE_FOAM for jellyroll material used by [11], MAT_24_PIECEWISE_LINEAR_PLASTICITY for steel casing used by [11] and MAT_20_RIGID for load; however for current collectors MAT_PLASTIC_KINEMATIC is used in [19]. Computation time using around 40000 elements with the element size of 0.8mm in [11] was 2.5 hrs; however with moderate element size in [19] with the total number of 108000 elements computation time was 8 hours for mechanical only simulation and 16 hours for coupled simulation. Figure 1, shows initial numerical simulation models from literature.

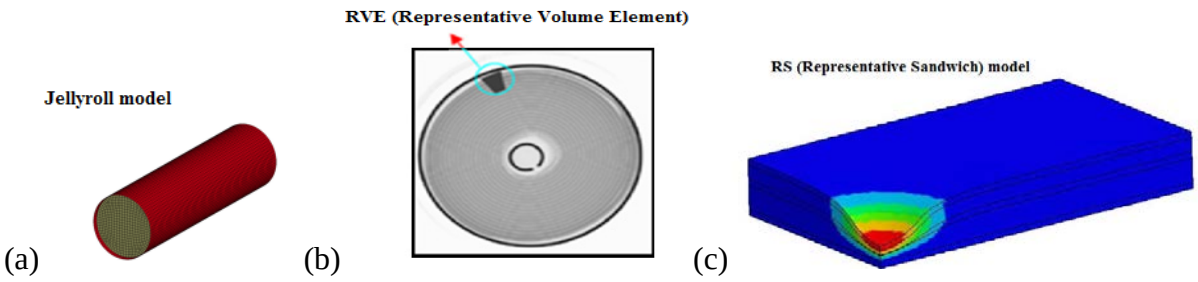

Figure 1: LS-DYNA numerical simulation models (a) Jellyroll model [11], (b) Representative volume element model [21], (c) Representative Sandwich model [19]

Thermal runaway detection strategies force-displacement, voltage-temperature, stress-strain, SOC dependency and separator failure discussed earlier are used in this paper. Separator failure is one of the indications of initial battery failure where due to the melting of separator layer contact can be established between active materials and current collectors of the battery.

2. Methodology

In this paper, both experimental and numerical simulation approaches are used to understand lithium-ion 18650 battery failures and various failure strategies are considered to detect signs of thermal runaway. Separator failure criteria given in [19] is investigated for two test protocols discussed later in this paper using numerical simulation model. Thermal analysis using infrared camera and thermocouples attached in different surface locations is carried to detect signs of thermal runaway. For thermal runaway detection temperature and voltage variations are important parameters in this regard.

2.1 Experimental approach

In this paper two sets of experiments are used, the first experiment is used for cell conditioning using charge, discharge and continuous monitoring of temperature and open circuit voltages (OCV), as voltage and temperature variations are important to understand short circuit induced thermal runaway. In the second experiment controlled chamber is designed using 3mm thick polycarbonate sheets to provide maximum protection to equipment and personnel. Calibrated mechanical press with load cell was used which is equipped with the data logger, thermal camera and laptop to capture and record data when different loading conditions are applied on initially conditioned cells.

2.2 Numerical simulation approach

For numerical simulation analysis of 18650 cylindrical lithium-ion battery, moderate number of elements are used. The size of the element varies as detailed in literature where element size of 0.25 to 0.8mm is found. In this paper element size for steel casing is 0.5mm and for all other layers is 1mm and this totals 103306 elements for single cell model and computation time for coupled mechanical and thermal analysis is 8 hours.

2.3 Validation of the model

To validate numerical simulation model comparison of structural deformation and temperature variations is conducted. Results for four test protocols discussed in experimental section are compared with numerical simulation results.

3. Description of experimental approach

Short circuit initiation is an important criterion to detect signs of thermal runaway in the case of mechanical abuse. Cells used in this work are Samsung 2200mAh lithium-ion cell from Samsung, Korea. The cell has dimensions of 18mm diameter and 65mm height. Low capacity cells were chosen to avoid severe conditions during cell conditioning and actual tests.

In this paper cell temperatures are not fixed, so the temperature variations are results of natural heat up and cool down. The cells were charged and discharged at three different C-rates 0.3C, 0.5C and 1C. Self-discharge was ignored due to the frequency at which the cells were used. To achieve accuracy and consistent results constant current (CC), constant voltage (CV) regime was used to condition all the cells used in this research. The discharge portion of the test cycle was performed at a constant current. The test protocol for each charge/discharge rate was as follows [24]:

1. Step 1 – Rest for 1 minute

2. Step 2 – Charging. The cell was charged at the specified rate until a cut off voltage was reached. This voltage was maintained until the current dropped to 0.01C (i.e. 22mA for these cells).

3. Step 3 – Discharge. The cells were discharged at the specified rate until the voltage dropped to cut off voltage.

4. Step 4 – Rest for 1 minute

The high rate of change of temperature causes sudden voltage drop which is evident in this research and discussed in detail concerning different abuse conditions. The temperatures are measured at three sites on the surface of each battery. The method of thermocouple attachment on the battery was implemented because it is a more practical method than, for example, the use of adiabatic Accelerating Rate Calorimetry (ARC) that requires access to an adiabatic calorimeter and causes gas release [5]. Attaching the thermocouples to three parts of the battery cell allowed the top, bottom and mid-surface battery sections to be evaluated for temperature changes [28]. Thermocouples are attached to the surface of each battery at the positive charge terminal end (+ve), the mid-surface and the negative charge terminal (-ve).

Battery testing protocols used in [11] is further investigated with the initial state of charge (SOC) and temperature variations where displacement, Force, temperature and voltage measurements are recorded after quasi-static loading is applied to the batteries.

Detailed experimental setup for mechanical loading is shown in figure 2, where all the equipment used with tests setup are shown. Quasi-static loading is used and loading speed was 1mm/min.

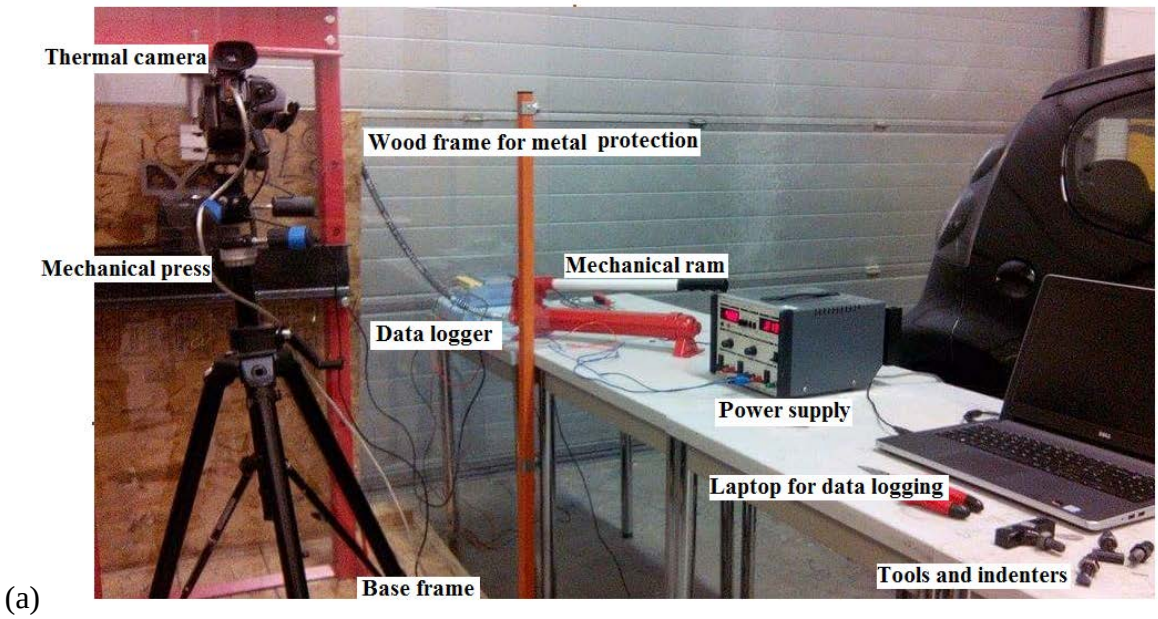

(a)

(b)

(c)

(d)

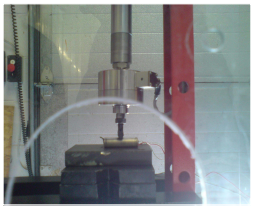

(e)

Figure 2: (a) Experimental setup for mechanical loading tests, (b) Flat plate, (c) Circular punch, (d) three-point bend (e) Rod test

The trials were run in five different SOCs (0%, 25%, 50%, 75% and 100%) to evaluate thermal runway of 18650 lithium ion battery cell at different SOCs. Authors in [11] also worked on 18650 lithium-ion batteries and SOC is kept constant at 10%, and temperature variations are not considered. In this work temperature variations concerning SOC is considered which varies at different loading conditions.

4. Description of numerical simulation approach

Based on above mentioned thermal and mechanical properties simulation model is designed to understand quasi-static loading on battery cell. For simulation, all layers (steel casing,

anode, cathode, separators, anode current collector and cathode current collector) are considered 0.3mm thick and inner most radius is considered 1mm as detailed in [29]. It is important to understand individual layers material properties for stress/strain relation and for that two foam material models discussed in [13] with compression and three-points bending test were considered for initial investigation. True stress/strain curve from dogbone specimen for shell casing is given in [6] and [20], nominal failure stress and failure strain are used from experimental results, and for each test case values at 0% SOC are used to check if the model predicts failure. Shell casing material is modelled using MAT-24-PIECEWISE-LINEAR-PLASTICITY in LS-DYNA. Separator, anode and cathode are considered as a MAT-63-CRUSHABLE-FOAM model, and anode current collector and cathode current collector are modelled using MAT-003-PLASTIC-KINEMATIC. Stress/strain curve for the separator, active anode material and active cathode material is used from [29] and [31]. Central core and cell terminals are not considered in this paper.

Concentric layer formation for the battery is used by Siva et al., as given in [29]. As cells have spiral wound formation in general, concentric layer model represents this structure, the main aim is to find an alternative way to model the battery and each layer is independent of other in the case of geometry, and layers share mechanical and thermal behaviours when the load is applied. Due to the higher number of elements used for this simulation, lowest termination time values are used. Parameters used for all layers in LS-DYNA simulation are taken from [11], [30][31] and given in table 1.

	Density (kgm^{-3})	Modulus of elasticity (MPa)	Heat capacity ($Jkg^{-1}K^{-1}$)	Thermal conductivity ($Wm^{-1}K^{-1}$)
Steel shell casing	*7830*	*200e5*	*477*	*14.9*
Separator	*1179*	*3.45e3*	*1978*	*0.334*
Anode active material	*2230*	*1e4*	*700*	*5*
Cathode active material	*4202*	*1e4*	*700*	*5*
Anode current collector	*7940*	*1.1e5*	*386*	*400*
Cathode current collector	*2699*	*7e4*	*900*	*200*

Table 1: 18650 cylindrical cell parameters for simulation [11][30][31]

Scaled layer thickness of each layer is chosen, where 0.1mm and 0.3mm thicknesses are found to be more accurate, but due to computation time results are concluded from 0.3mm thick layers. Layers properties are used form experimental work and literature.

5. Results and Discussion

This section provides detail results obtained from experimental test and numerical simulation and validation of results.

5.1 Mechanical failure due to loading

To understand mechanical failures, force-displacement and voltage-temperature response due to loading are observed, and failure pattern is closely monitored which indicate short circuit initiation and thermal runaway as the temperature increase in the short period and cells undergo permanent damages. Detailed results are given in this section.

5.1.1 Short circuit initiation

short circuit occurrence was reported immediately at the point where due to initial contact indication of cell failures in the form of voltage drop and temperature rise occurs.

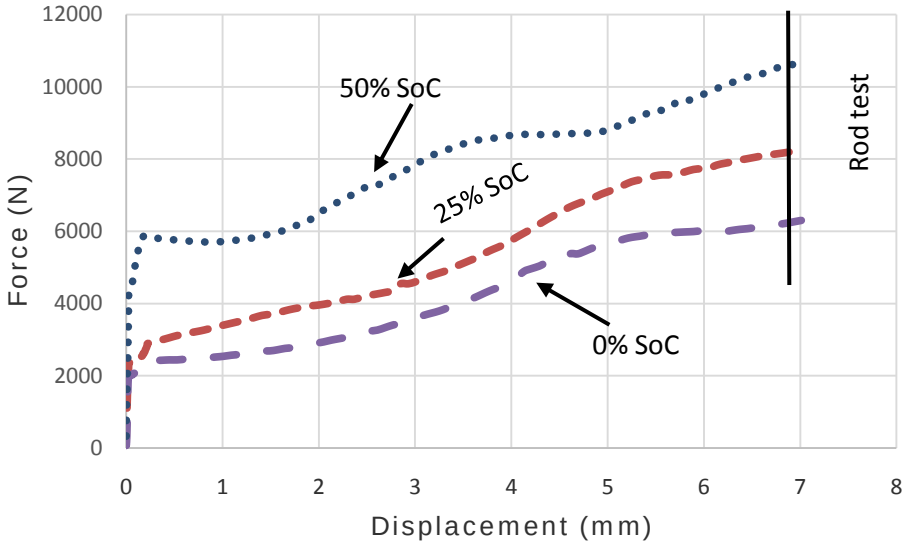

(a)

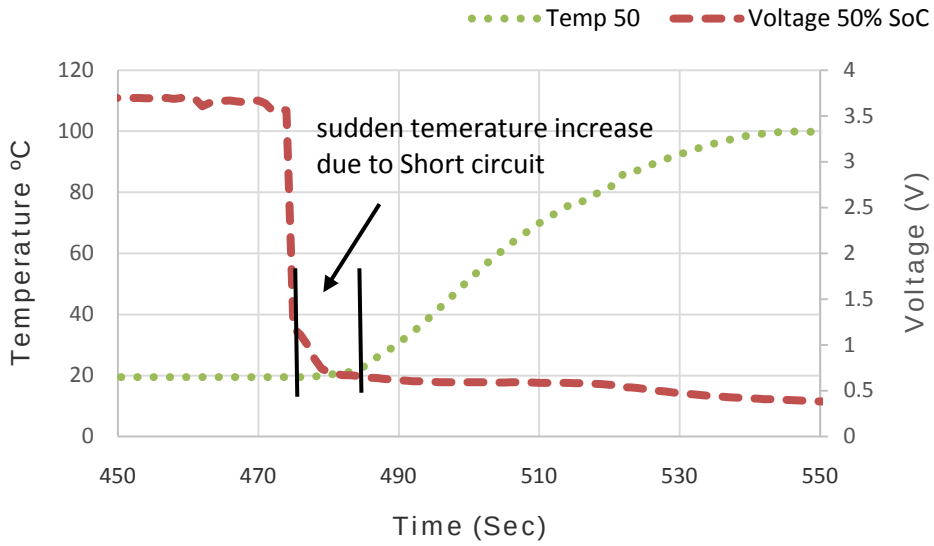

(b)

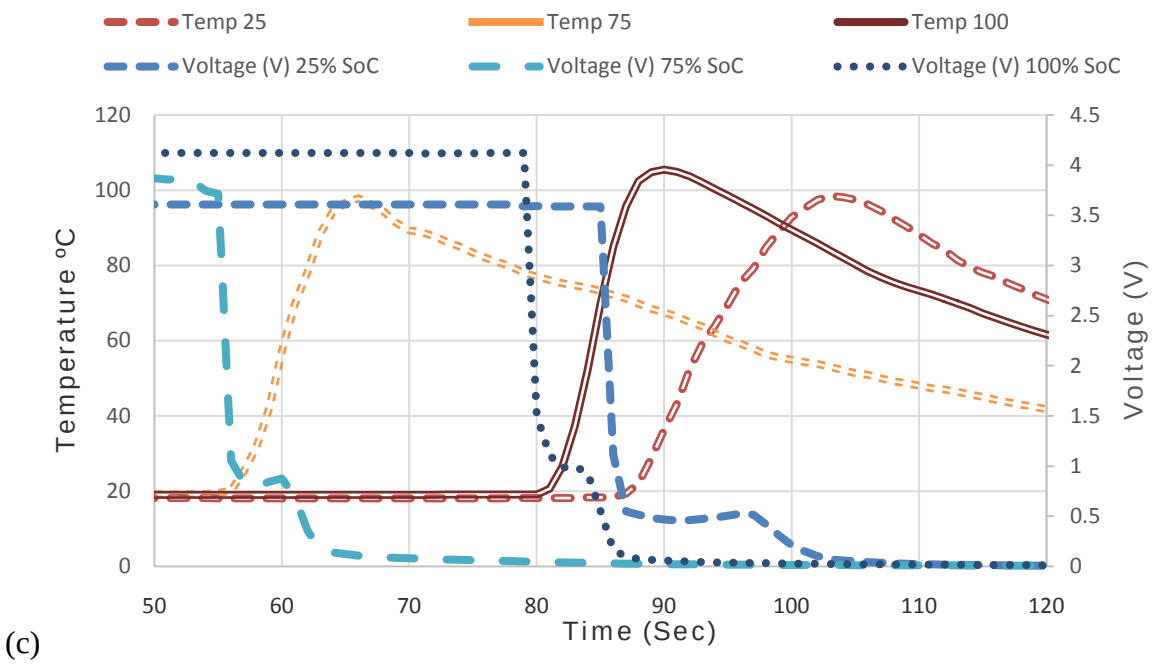

(c)

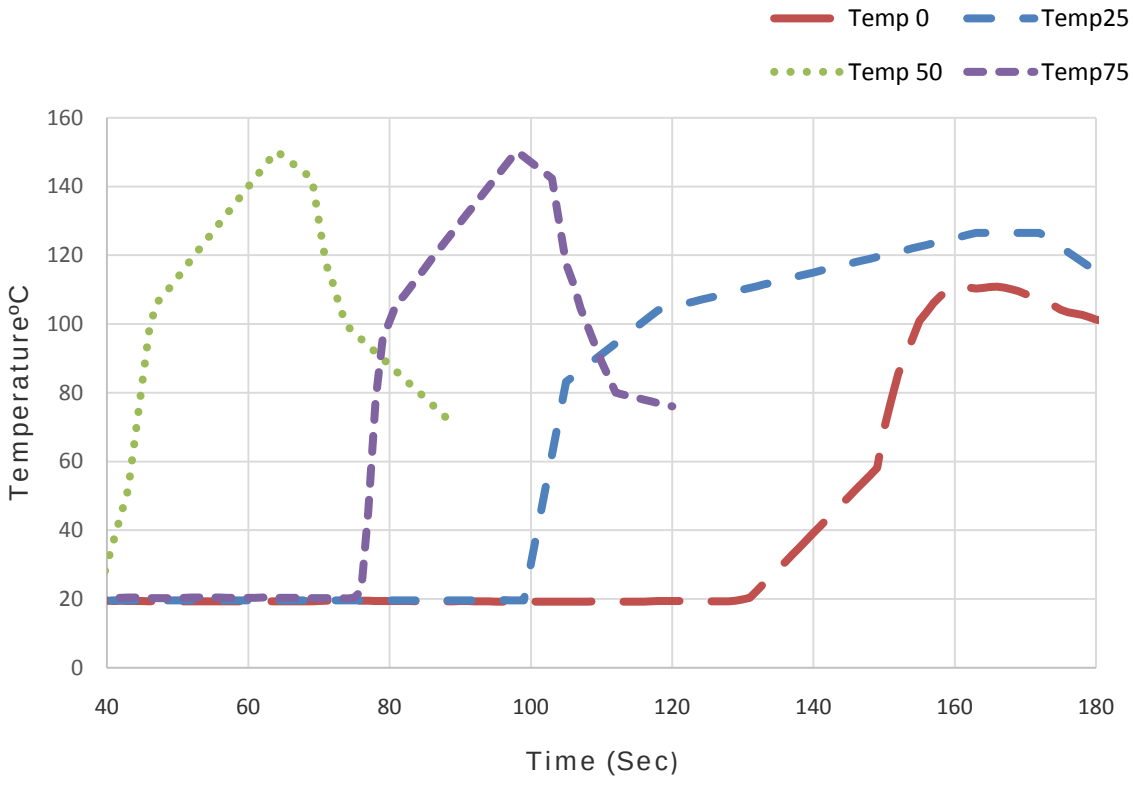

(d)

Figure 3: (a) Rod test, force and displacement at different SOCs (b) Short circuit occurrence at 50% SOC due to circular punch, (c) Three-point bend, voltage and temperature relation, (d) Flat plate temperature variations at various SOC

As shown in figure 3, the displacement varies at various SOCs therefore to generalize results and achieve accuracy, displacement cut off point was set to 6.94mm which is average displacement as given later in this section. At the point when force starts to decrease short circuit occurrence is reported as less force is required to deform internal layers of the cell.

Force vs. displacement and voltage vs. temperature, for all test scenarios, is presented, most of the batteries appear to have experienced short circuit followed by temperature increases, except for the 0% SOC Circular Punch test. Voltage drop was significant to mention failures.

As shown in figure 3 (d), for flat plate deformation, temperature variations at low SOCs is slow to build-up compare to high SOCs where significant change is observed and attain high values immediately after the short circuit.

There appear to be two major patterns; the first where the temperature increase occurs as the voltage drops, and the second where the voltage drop precedes the temperature increase. In some of the cases temperatures only rise a few degrees to the mid 30ºC from the initial room temperature starting point (approximately 20ºC), but in general, temperatures spiked at above 100ºC. Flat plate failures appear to have the highest temperature increases of all the failure scenarios tested. It appears that most failures occur after 5-7 minutes of loading, but longer periods exist for some tests. Table 2, shows mean displacement for each loading condition and standard deviation of displacement.

Loading condition	Mean Displacement	Std. Deviation of Displacement
Three-point	*7.272*	*1.083*
Circular Punch	*7.571*	*0.287*
Flat Plate	*6.036*	*0.971*
Rod indentation	*6.900*	*1.731*
ALL	*6.945*	*1.202*

Table 2: Mean displacement at short circuit

The average displacement that began short circuit was 6.94mm, and it appears that flat plate deformation tests developed short circuit earlier compare to other loading conditions and for this case mean displacement is nearly 6mm, this finding is similar to the displacement observed by [11] who also tested indentation on 18650 lithium ion cells. In [11], authors observed that displacement greater than approximately 6.5 mm was associated with the outer shell of the casing fracturing and followed by the jelly roll fracturing internally and initiation of the short circuit.

5.1.2 Nominal stress-strain behaviour

Nominal stress and nominal strain behaviors are calculated using Eq. 1 as follows,

$$\sigma_n = \frac{F}{A} \tag{1}$$

"F" is the force applied as shown and discussed in this chapter and previous chapter, "A" is the area of contact as given in [7] as follows,

$$\mathrm{A} = l_c b_c \tag{2}$$

"l_c" is the length of the cell and width of the contact b_c was calculated by Eq. 3, as given below,

$$b_c = 2Rarc\,cos\left[\frac{R-s/2}{R}\right] \tag{3}$$

"R" is the radius of the cell and "s" is the displacement of the indenter used, so the nominal stain ε_n can be obtained using Eq. 4, given as follow

$$\varepsilon_n = \frac{s}{2R} \tag{4}$$

Compression modulus for flat plate deformation (E_{cf}) is also calculated and found that occurrence of short circuit is the point where cell failure start to develop and for this test E_{cf} is 205MPa. For rod test, failure strain showed linear relationship and had adjusted R square fit of 0.8449, as shown in figure 4, "ε_{fr}" represents failure strain for rod indentation test.

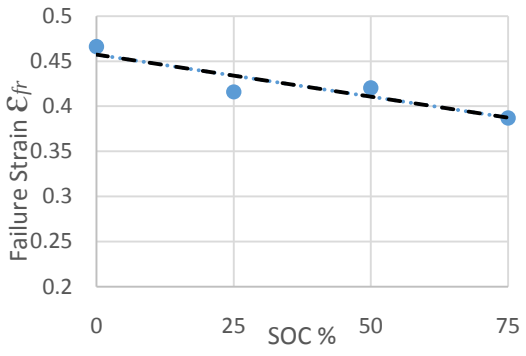

(a)

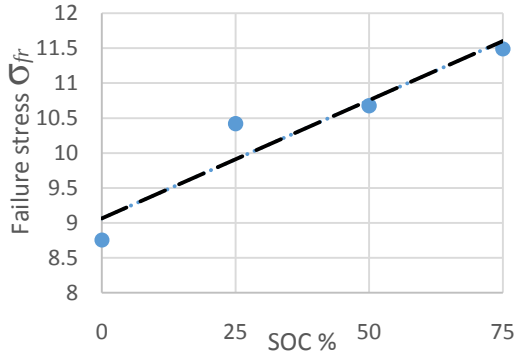

(b)

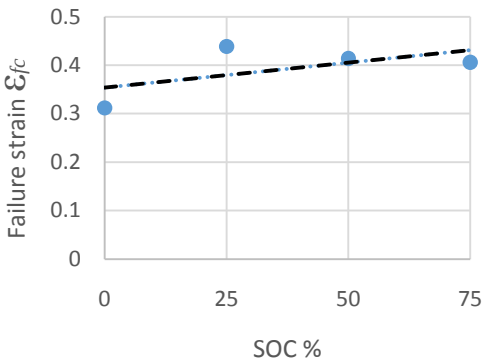

(c)

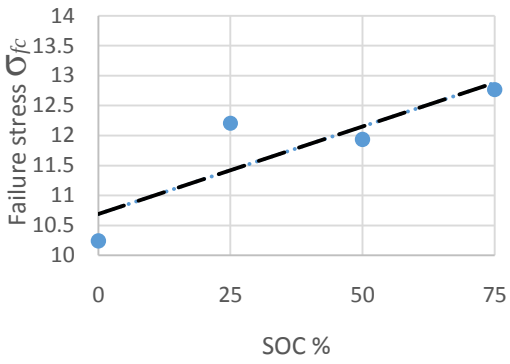

(d)

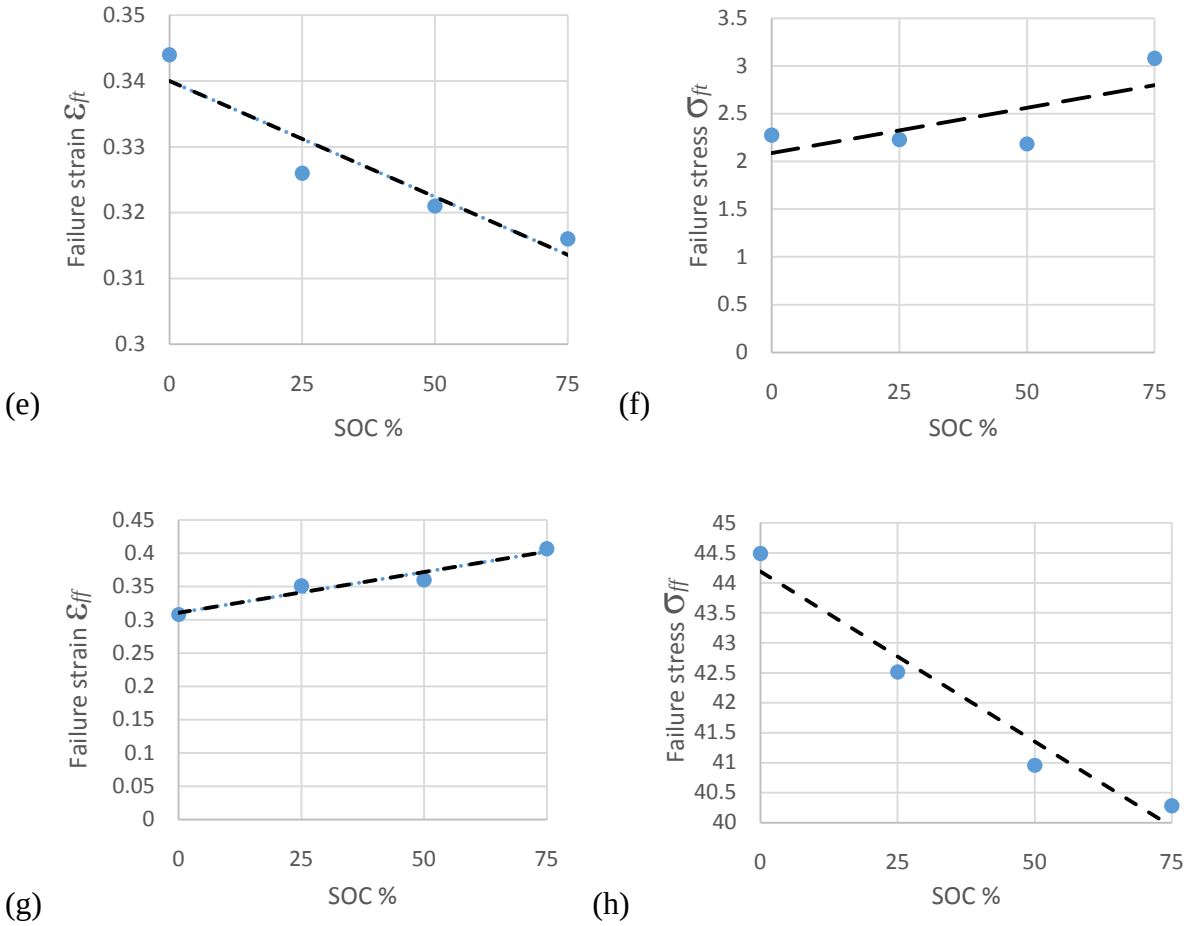

Figure 4: (a) Rod test, nominal failure strain, (b) Rod test, nominal failure stress (c) Circular punch test, nominal failure strain ,(d) Circular punch test, nominal failure stress, (e) Three point bending test, nominal failure strain, (f) Three point bending test, nominal failure stress (g) Flat plate deformation test nominal failure strain (h) Flat plate deformation test nominal failure stress

Governing equation due to linear fit for failure strain and failure stress are given as follows,

$$\varepsilon_{fr} = 0.4573 - 0.0009\text{SOC} \tag{5}$$

$$\sigma_{fr} = 9.065 + 0.0339\text{SOC} \tag{6}$$

Eqs. (5) and (6) can be used for rod test failure strain and stress respectively, where "ε_{fr}"

represents failure strain, and "σ_{fr}" represents failure stress for rod test. With the increasing SOC failure stress increases and directly link to the electrochemical behaviour of cells where cell stiffness increases as SOC increases, this is in agreement with the researches from [7] and [11].

Governing equations for circular punch failure strain and failure stress are as follows,

$$\varepsilon_{f_c} = 0.354 + 0.001\text{SOC} \tag{7}$$

$$\sigma_{fc} = 10.691 + 0 \cdot 0292\text{SOC} \tag{8}$$

To better understand and generalize cell failure due to three-point bending, failure strain for three point bending test is shown in figure 4(e).

$$\varepsilon_{ft} = 0.34 - 0.0004\text{SOC} \tag{9}$$

$$\sigma_{ft} = 2.0872 + 0.0095\text{SOC} \tag{10}$$

Eqs. (9) and (10), shows linear fit for three point bending "ε_{ft}" represents failure strain and σ_{ft} represents failure stress for three point bending test.

Linear fit for flat plate deformation was obtained and adjusted R square was 0.9468. Like circular punch test flat plate deformation had linearly increasing response, with increasing SOC failure strain has highest values. Eqs. (11) and (12) provide linear fit for flat plate deformation.

$$\varepsilon_{ff} = 0 \cdot 3106 + 0.0012\text{SOC} \tag{11}$$

$$\sigma_{ff} = 44.188 - 0.0567\text{SOC} \tag{12}$$

ε_{ff} represents nominal failure strain, and σff represents failure stress for flat plate deformation.

From failure stress and failure strain for all loading conditions, it can be concluded that failure stress and failure strain at 25% and 50% SOCs have identical values for individual tests, except flat plate deformation where failure stress is linearly decreasing with increasing SOC.

5.2 Numerical simulation analysis

Parameters obtained from experimental work and available literature are used for the numerical simulation model, nominal strain failure and heat transfer between layers is considered by using parameters in contact cards as detailed in earlier sections. Results obtained from numerical simulation are discussed in this section.

5.2.1 Structural failure analysis

Structural failure analysis is conducted using LS-DYNA numerical simulation tool in this analysis simulation models show good correlation with experimental work as shown in figure 5.

(a)  (b) 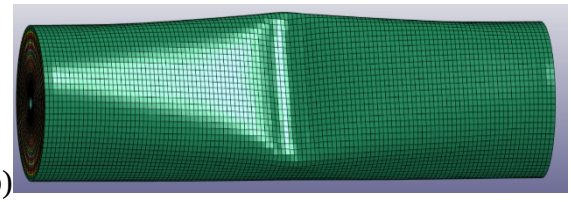

(c)  (d) 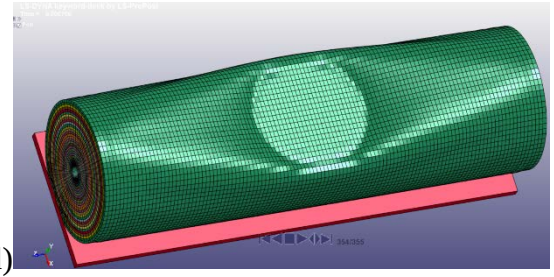

(e)  (f) 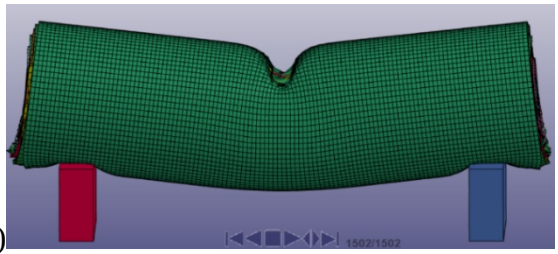

(g) 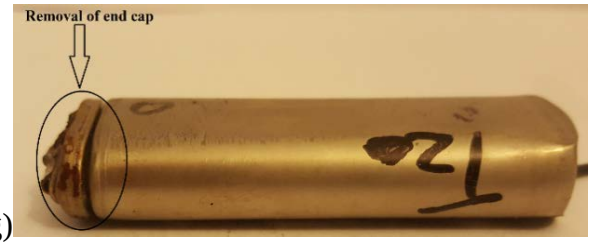

(h) 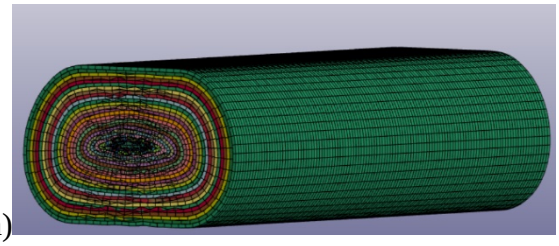

Figure 5: Deformed cells and simulation model, (a) Rod test, (b) rod simulation, (c) Circular punch test, (d) Circular punch simulation, (e) Three point bend test, (f) Three point bend simulation, (g) Flat plate test, (h) Flat plate simulation

Each simulation model shows similar deformation pattern as observed in experimental work, and the force-displacement relationship is also in good correlation with test protocols. Temperature variations for all test protocols are observed for validation of results.

5.2.2 Temperature variations

Temperature cut off is considered when the temperature started to change from the initial value, and indicates short circuit occurrence. Temperature variations for surfaces of cells for rod test, circular punch, flat plate deformation and three-point bending are as follows.

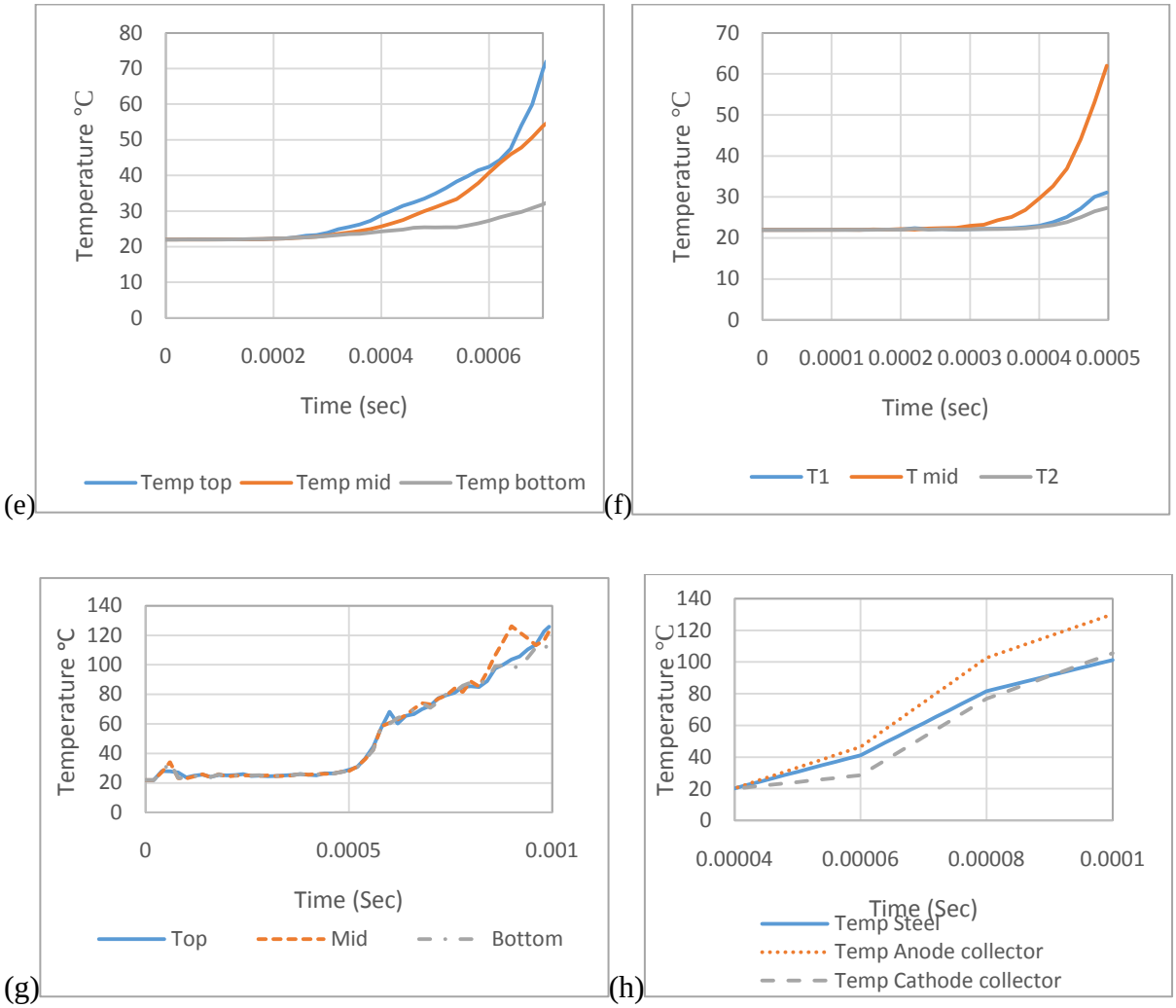

Figure 6: Numerical simulation results for temperature variations due to short circuit, (a) Circular punch, (b) Rod test, (c) Flat plate, (d) Three-point bending

High-temperature increase due to the short circuit and sample time for temperature increase is shown in figure 6. Uncontrolled temperature within the short instance of time indicates thermal runaway occurrence as voltage drop is also observed at this point.

6. Validation of simulation model

To validate short circuit initiation concerning separator layer temperature variations, further analysis was carried out on circular punch and three-point bending numerical simulation model. Separator layers have the lower melting point in lithium ion battery construction, it can melt at around 144°C [19], and so separator failure can occur earlier compare to other layers failure as separator layers have comparatively high temperatures.

(A)

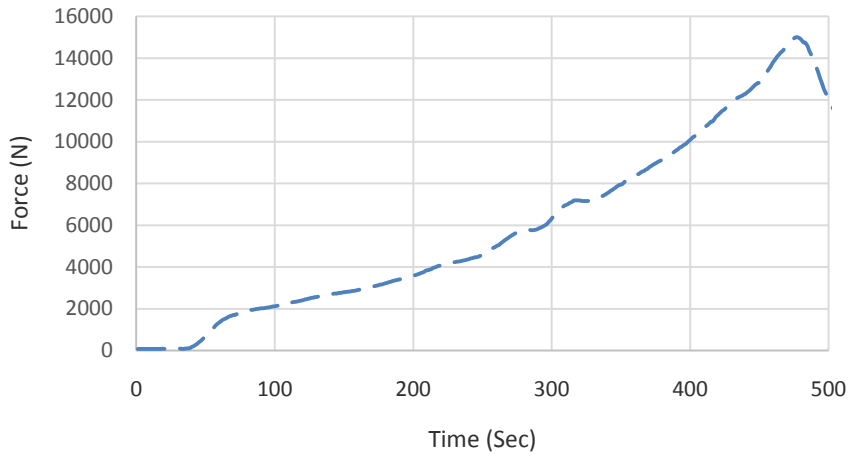

(i)

(ii)

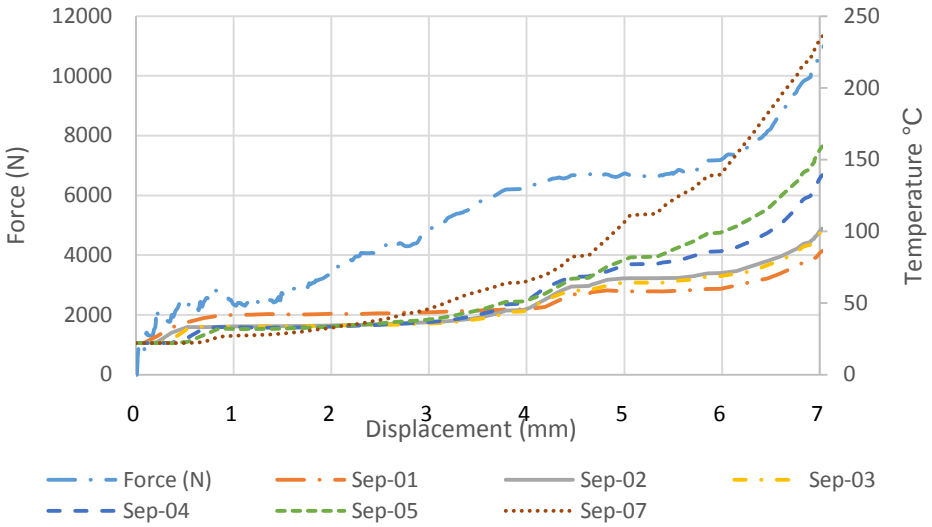
12000
10000
8000
6000
4000
2000
0
Force (N)
250
200
150
100
50
0
Temperature °C
0
1
2
3
4
5
6
7
Displacement (mm)
Force (N)
Sep-01
Sep-02
Sep-03
Sep-04
Sep-05
Sep-07

(B)

(i)

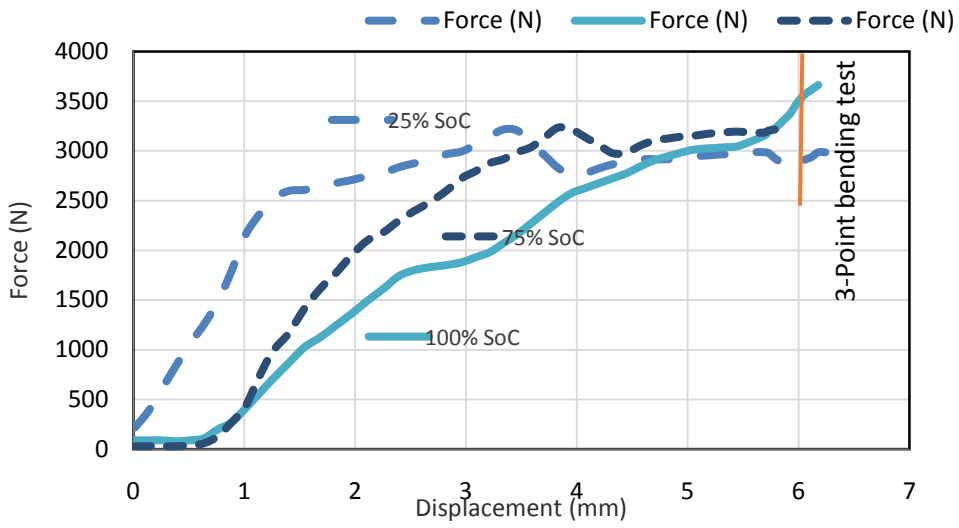
Force (N)
Force (N)
Force (N)
4000
3500
3000
2500
2000
1500
1000
500
0
Force (N)
25% SoC
75% SoC
100% SoC
3-Point bending test
0
1
2
3
4
5
6
7
Displacement (mm)

(ii)

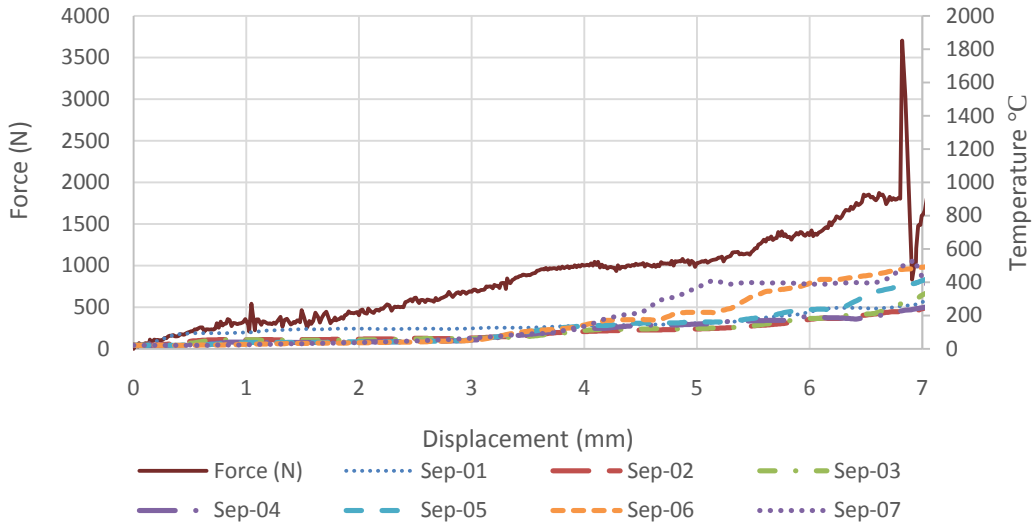

Figure 7: (A) Circular punch test, (i) Experimental results for applied force at 0% SOC, (ii) simulation results for separator layers (B) Three-point bend, (i) Applied force for various SOCs, (ii) Simulation results for separator layers

As can be seen from figure 7(A), the force applied has same pattern and values are within 10% of experimental values. In separator temperature variations, first five separator layers showed temperature variations well within the safe zone of separator melting point is mentioned in [19], however last two layers showed high temperatures and exceeds melting point, this illustrates the beginning of permanent cell failures as initial failures occurred at the time of short circuit and due to deformation cell temperature increased. Identical displacement values for experimental results and simulation results at the time of short circuit support this analysis.

Simulation model results show good accuracy with the experimental results comparison. As shown in figure 7(B), force attains the same peak value as in experimental work, a sudden drop in force at around 7mm shows the point of short circuit occurrence. The difference between applied force and values in the simulation may be due to 0% SOC is used for the numerical simulation model. Temperatures of all layers started to increase after short circuit

and the last separator layer “sep-07”, experiences temperature drop and indicate stabilising zone or short circuit propagation. Once the thermal runaway occurs temperature started to increase in uncontrolled manner, and temperature of all layers were around 300°C except sep-05 to sep-07 which attain temperatures of around 500°C for short instant of time. Sep-07 layer experience high compression and tension due to three-point bend as forces from all other layers and indenter are applied at this layer, due to this layer shrink and element deletion takes place. Separator analysis with high-temperature variations can be used as an indicator of cell failure, and is evident from the literature but FEA of the cell for this analysis is not found in detail. Separator temperature variations above melting point are the good indicator of short circuit and it can lead to thermal runaway if the temperature of other separator layers increases.

7. Indication of thermal runaway

To understand the permanent damage to the cell, two cells were chosen randomly from all tested cells. All cells experience short circuit and undergo thermal runaway, and electrical, mechanical and thermal properties change. Cells with the unusual response for all test scenarios are chosen to investigate for remaining capacity in this section, and initially low C-rate is applied, and then high C-rate of up to 1C is applied to check either cell undergo sleeping mode or permanent damage condition. Results and respective observations are discussed in detail. Like in rod test only 0% and 50% initially tested SOC cells were in good

condition without any crack which was appropriate to carry out the further experiment. Circular punch 0% SOC damaged the cell and flat plate 25% SOC damaged cells showed excellent charge-discharge behaviour after post-failure assessment, however other cells started to charge as 1C charge current (2.2A) was applied, but after some time, they started to loose charge and temperature increment was noticed. They were removed from charger to observe variations and slow voltage drop is observed which shows severe internal damages occurred in these cells and not allow to charge transfer and these damages are impossible to revert however due to heat capacity and thermal conductivity characteristics it is still possible that these sufficiently damaged cells can contribute towards the temperature increase of adjacent cells in the pack because battery terminals are still in good shape and may behave same in these events unless they come under crash zone in particular loading direction. Figure 8, shows tested cells, with respective voltage and temperature variations.

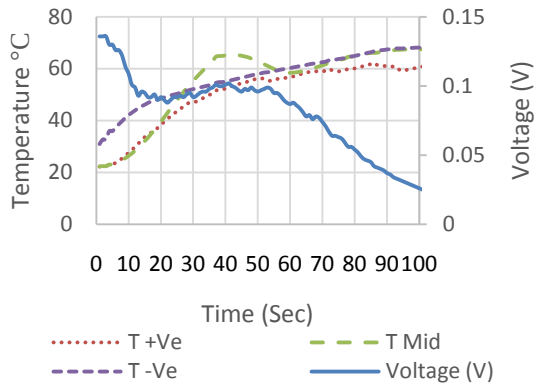

(a)

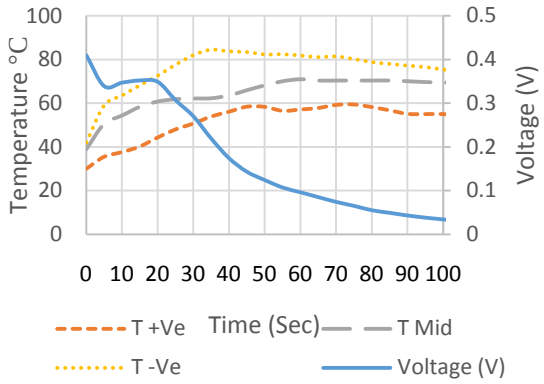

(b)

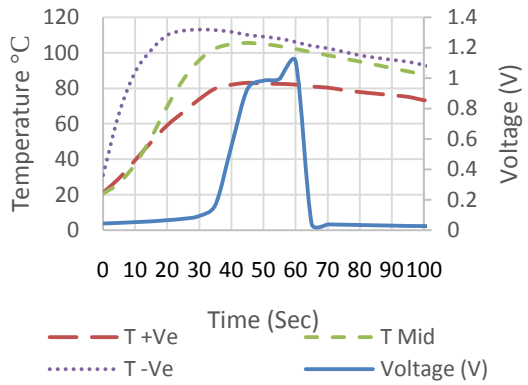

(c)

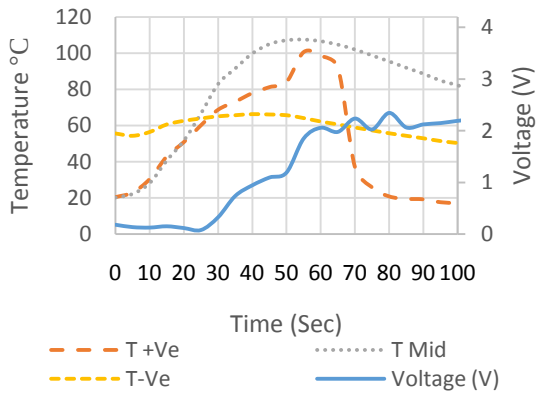

(d)

Figure 8: (a) Rod test, damaged cell with 50% SOC, (b) Circular punch test, damaged cell with 0%SOC, (c) Three-point bend test, damaged cell with 75% SOC, (d)Flat plate test, damaged cell with 25% SOC

Interesting results are achieved for these tests as for circular punch and rod tests, cells show similar voltage and temperature curves, and temperature values at each surface location are similar and show similar curve response. Voltage increases for short period of time and slowly decreases to zero and shows cells are completely damaged and cannot hold the charge, however at the low charge current these cells show the same response.

For flat plate and three point bend test, cells start to hold the charge for short period of time but after some time while connected to power supply they started to discharge, and high ripples are observed in flat plate test, this analysis shows internal electrochemical discrepancy due to damages. Maximum temperatures for both tests were above 100˚C and slowly drop down to ambient temperature.

8. Conclusions

The objective of the current research was to successfully investigate thermal runaway of 18650 lithium-ion batteries. Quasi-static loading conditions were applied to cause displacement over time accompanied with voltage measurements. The methodology is shown to work well by comparing the thermal changes. The current research demonstrated that the method offers a reliable and efficient way to study thermal runaway in lithium ion batteries under different scenarios of SOCs. The outputs of displacement and time duration were found to show a correlation. Temperature increase rate of up to 700°C was observed and sudden voltage drop and temperature rise indicates the occurrence of short circuit. Temperature variations at different surface locations, especially at the point of impact shows the effectiveness of using various loading conditions to detect early signs of thermal runaway.

The results are far more dramatic for the flat plate compression than for the rod caused displacement, however, three points bend showed instant failure behaviour and casing fracture. Numerical simulation models show good correlation with experimental work and all the results for temperature variations and applied force are well within 10% of experimental results. Separator failure analysis for thermal runaway detection can be a good choice for large battery pack failures where due to the increase of every degree of temperature chances of thermal runaway in individual cell and battery pack becomes high and result in battery degradation or permanent failures.

Acknowledgments

The authors would like to acknowledge the support of all the staff at the Automotive and Manufacturing Advanced Practice (AMAP), university of Sunderland, UK, and also special thanks to Brian Britton, from Gestamp ltd. Gateshead, UK for lending load cell for this research.

9. References

[1] Chanson, C., J-P Wiaux. “Safety of Lithium Batteries”, RECHARGE aisbl, pp. 1-26, June 2013.

[2] Golubkov, A. W., Fuchs,, D., Wagner, J., Wiltsche, H., Stangl, C. Fauler, G., Voitic, G., Thaler, A and Hacker , V. 2014.Thermal-runaway experiments on consumer Li-ion batteries with metal-oxide and olivin-type cathodes. RSC Adv., 4: 3633-3642.

[3] Finegan, D. P., Scheel, M,. Robinson1, J. B., Tjaden, B. Hunt, I., Mason1, T. J.,

Millichamp, J., Di Michiel, M., Offer, G. J., Hinds, G., Brett, D. J. L. and & Paul, R. Shearing. 2015. In-operando high-speed tomography of lithium-ion batteries during thermal runaway. Nature Communications, 6:6924, 10 pp., doi: 10.1038/ncomms7924

[4] Yong Xia, Tomasz Wierzbicki, Elham Sahraei, Xiaowei Zhang, Journal of Power Sources 267 (2014) 78-97.

[5] Orendorff, C. .J., Lamb, J., Steele, L-A., M., Spangler, S.W. and Langendorf, J. 2016. “Quantification of Lithium-ion Cell: Thermal Runaway Energetics” SANDIA REPORT, Report No.SAND2016-0486, 49 pp.

[6] Chao Zhang, Shriram Santhanagopalan, Michael A. Sprague, Ahmad A. Pesaran, Journal of Power Sources 290 (2015) 102-113.

[7] Xu, J., Liu, B., Hu, D., 2016. Sci. Rep. 6, 21829; doi: 10.1038/srep21829 (2016).

[8] Thermal Runaway Risk Assessment by Mechanically Induced Internal Short Circuit”, Hsin Wang and Edga Lara-Curzio (Oak Ridge National Laboratory, Oak Ridge, TN), Clint Winchester, Evan Rule, Jacob Helmer (Naval Surface Warfare Center, Carderock, MD), Projects supported by DOE EERE VTP and NHTSA, DOE, January 2017, http://www.prba.org/wp-content/uploads/Internal-short-circuit-BatterySafetyCouncil-Jan2017.pdf (Accessed on April 2017).

[9] Hsin Wang, Edgar Lara-Curzio, Evan T. Rule, Clinton S. Winchester, J. Power Sources 342 (2017), pages 913-920.

[10] Sahraei, E., Emanuela Bosco, Brandy Dixon, Benjamin Lai, J. Power Sources, Volume 319, 1 July 2016, Pages 56-65.

[11] Sahraei, E., John Campbell, Tomasz Wierzbicki, J. Power Sources, Volume 220, 15 December 2012, Pages 360-372, ISSN 0378-7753,

[12] Sahraei, E., Joseph Meier, Tomasz Wierzbicki. J. Power Sources, Volume 247, 1 February 2014, Pages 503-516.

[13] Gerhard Slik, Gavin Vogel and Virendra Chawda, “Material model validation of a high efficient energy absorbing foam”, 5th LS-DYNA forum, Ulm 2006.

[14] Y. Bai, X. Teng, T. Wierzbicki, J. Eng. Mater. Technol. 131 (2009) 021002.

[15] Doughty, D., "SAE J2464 “EV & HEV Rechargeable Energy Storage System (RESS) Safety and Abuse Testing Procedure”," SAE Technical Paper 2010-01-1077, 2010, doi:10.4271/2010-01-1077.

[16] WenWei WANG, Sheng YANG, Cheng LIN, Energy Procedia 104 (2016) 56 – 61.

[17] Jingjing Liu, Zhirong Wang, Junhui Gong, Kai Liu, Hao Wang and Linsheng Guo, Materials 2017, 10, 230; doi:10.3390/ma10030230.

[18] Elham Sahraei, Michael Kahn, Joseph Meierc and Tomasz Wierzbicki, RSC Adv., 2015, 5, 80369.

[19] Chao Zhang, Shriram Santhanagopalan, Michael A. Sprague, Ahmad A. Pesaran, J. Power Sources 298 (2015), pages 309-321.

[20] Sahraei, E., Rich Hill, Tomasz Wierzbicki, J. Power Sources, Volume 201, 1 March 2012, pages 307-321.

[21] Elham Sahraei, Joseph Meier, Tomasz Wierzbicki, J. Power Sources 247 (2014), pages 503-516.

[22] Marco Raffler, Alessio Sevarin, Christian Ellersdorfer, Simon F. Heindl, Christoph Breitfuss, Wolfgang Sinz, J. Power Sources 360 (2017), pages 605-617.

[23] M. Funcke, S. Schäfer, R. Wohlecker, D. Dufaut, D. Sturk, K. Vavalidis, D3.15 Report on validation of FE simulations of WT3.1, 11th March 2014.

[24] Sheikh, M., Baglee, D., Knowles, M., Elmarakbi, A., Al_Hariri, M., “A Novel Approach for Predicting Thermal Runaway in Electric Vehicle Batteries When Involved in a Collision” ASME 2015 International Mechanical Engineering Congress and Exposition, Volume 12: Transportation Systems, doi:10.1115/IMECE2015-51781.

[25] Jun Xu, Binghe Liu & Dayong Hu, Sci. Rep. 6, 21829; doi: 10.1038/srep21829 (2016).

[26] Y. Bai, T. Wierzbicki, Int. J. Mech. Sci. 50 (2008) 1012-1022.

[27] James Marcicki, Min Zhu, Alexander Bartlett, Xiao Guang Yang, Yijung Chen, Theodore Miller, Pierre L’Eplattenier, and I ˜naki Caldichoury, Journal of The Electrochemical Society, 164 (1) A6440-A6448 (2017).

[28] Sahraei, E., Emanuela Bosco, Brandy Dixon, Benjamin Lai, J. Power Sources, Volume 319, 1 July 2016, Pages 56-65

[29] Siva P.V. Nadimpalli, Vijay A. Sethuraman, Daniel P. Abraham, Allan F. Bower, Pradeep R. Guduru, J. Electrochemical Society, 162 (14), A2656-A2663, 2015.

[30] Chao Zhang, Shriram Santhanagopalan, Michael A. Sprague, Ahmad A. Pesaran, J. Power Sources 290 (2015), pages 102-113.

[31] http://www.engineeringtoolbox.com/young-modulus-d_417.html (Accessed on May 2017)